POSIVA 99-21

Ion diffusion in compacted bentonite

Jarmo Lehikoinen
VTT Chemical Technology

March 1999

POSIVA OY
Mikonkatu 15 A, FIN-00100 HELSINKI, FINLAND
Phone (09) 2280 30 (nat.), (+358-9-) 2280 30 (int.)
Fax (09) 2280 3719 (nat.), (+358-9-) 2280 3719 (int.)

Posiva-raportti – Posiva Report

Posiva Oy
Mikonkatu 15 A, FIN-00100 HELSINKI, FINLAND
Puh. (09) 2280 30 – Int. Tel. +358 9 2280 30

Raportin tunnus – Report code
POSIVA 99-21

Julkaisuaika – Date
March 1999

Tekijä(t) – Author(s)

Jarmo Lehikoinen
VTT Chemical Technology

Toimeksiantaja(t) – Commissioned by

Posiva Oy

Nimeke – Title

ION DIFFUSION IN COMPACTED BENTONITE

Tiivistelmä – Abstract

In this study, a two-dimensional molecular-level diffusion model, based on a modified form of the Gouy-Chapman (GC) theory of the electrical double layers, for hydrated ionic species in compacted bentonite was developed. The modifications to the GC theory, which forms the very kernel of the diffusion model, stem from various non-conventional features: ionic hydration, dielectric saturation, finite ion-sizes and specific adsorption.

The principal objectives of the study were met. With the aid of the consistent diffusion model, it is a relatively simple matter to explain the experimentally observed macroscopic exclusion for anions as well as the postulated, but greatly controversial, surface diffusion for cations. From purely theoretical grounds, it was possible to show that the apparent diffusivities of cations, anions and neutral molecules (i) do not exhibit order-or-magnitude differences, and (ii) are practically independent of the solution ionic strength used and, consequently, of the distribution coefficient, K_d, unless they experience specific binding onto the substrate surface.

It was also of interest to investigate the equilibrium anionic concentration distribution in the pore geometry of the GMM model as a function of the solution ionic strength, and to briefly speculate its consequences to diffusion.

An explicit account of the filter-plate effect was taken by developing a computerized macroscopic diffusion model, which is based upon the very robust and efficient Laplace Transform Finite-Difference technique.

Finally, the inherent limitations as well as the potential fields of applications of the models were addressed.

Avainsanat - Keywords

Diffusion, ion, bentonite, montmorillonite, compacted, electrical double layer, equilibrium, hydration, adsorption, exclusion

ISBN	ISSN
ISBN 951-652-076-6	ISSN 1239-3096
Sivumäärä – Number of pages: 37	Kieli – Language: English

Posiva-raportti – Posiva Report

Posiva Oy
Mikonkatu 15 A, FIN-00100 HELSINKI, FINLAND
Puh. (09) 2280 30 – Int. Tel. +358 9 2280 30

Raportin tunnus – Report code
POSIVA 99-21

Julkaisuaika – Date
Maaliskuu 1999

Tekijä(t) – Author(s)

Jarmo Lehikoinen
VTT Kemiantekniikka

Toimeksiantaja(t) – Commissioned by

Posiva Oy

Nimeke – Title

IONIEN DIFFUUSIO KOMPAKTOIDUSSA BENTONIITISSA

Tiivistelmä – Abstract

Työssä kehitettiin kaksiulotteinen molekyylitason diffuusiomalli hydratoituneille ioneille, joka perustuu modifioituun Gouy-Chapmanin (GC) teoriaan sähköisestä kaksoiskerroksesta. Modifikaatiot GC teoriaan, joka muodostaa varsinaisen diffuusiomallin ytimen, aiheutuvat monista epäkonventionaalisista piirteistä: ionien hydratoitumisesta, dielektrisestä saturaatiosta, äärellisestä ionikoosta sekä spesifisestä sorptiosta.

Työn ensisijaiset päämäärät saavutettiin. Konsistentin diffuusiomallin avulla on suhteellisen helppo selittää kokeellisesti havaittu anioniekskluusio sekä oletettu, mutta erittäin kiistanalainen, kationien pintadiffuusio. Täysin teoreettisista lähtökohdista käsin on mahdollista osoittaa, että kationien, anion sekä neutraalien molekyylien näennäiset diffuusiokertoimet ovat (i) samaa suuruusluokkaa ja (ii) käytännöllisesti katsoen riippumattomia liuoksen ionivahvuudesta ja jakautumiskertoimesta, K_d, elleivät ne adsorboidu spesifisesti väliaineen pinnalle.

Oli myös kiinnostavaa tutkia anionien tasapainopitoisuusjakaumaa GMM-mallin mukaisessa huokosgeometriassa liuoksen ionivahvuuden funktiona ja lyhyesti spekuloida sen vaikutuksia diffuusioon.

Työssä otettiin eksplisiittisesti huomioon myös sintterilevyefekti kehittämällä tietokoneistettu makroskooppinen diffuusiomalli, joka perustuu erittäin robustiin ja tehokkaaseen "Laplace Transform Finite-Difference" -tekniikkaan.

Lopuksi esiteltiin mallien rajoituksia sekä mahdollisia sovelluskohteita.

Avainsanat - Keywords

Diffuusio, ioni, bentoniitti, montmorilloniitti, puristettu, sähköinen kaksoiskerros, tasapaino, hydratoituminen, adsorptio, ekskluusio

ISBN	ISSN
ISBN 951-652-076-6	ISSN 1239-3096
Sivumäärä – Number of pages: 37	Kieli – Language: Englanti

TABLE OF CONTENTS

page

ABSTRACT

TIIVISTELMÄ

PREFACE

1 INTRODUCTION ... 3

2 FROM MICROSCOPIC THEORY 5
2.1 Modified Gouy-Chapman (MGC) theory ... 5
2.2 Specific adsorption on a charge-regulated surface ... 7
2.3 Diffusion ... 9

3 ... TO MACROSCOPIC THEORY ... 13
3.1 Adsorption ... 13
3.2 Diffusion ... 15

4 RESULTS AND DISCUSSION ... 18
4.1 Ionic equilibria ... 18
4.1.1 MGC theory ... 18
4.1.2 Specific adsorption ... 21
4.1.3 GMM geometry ... 22
4.2 Diffusion ... 25
4.2.1 General considerations ... 25
4.2.2 Theoretical results ... 26
4.2.3 Effect of filter-plates and the LFD code ... 30
4.2.4 Pore size in compacted bentonite ... 32
4.3 Limitations and applications ... 33

5 REFERENCES ... 35

PREFACE

Within the European Commission Nuclear Fission Safety Programme (1994–1998), the research project "Microstructural and Chemical Parameters of Bentonite as Determinants of Waste Isolation Efficiency" (Contract No. FI4W-CT95-0012) was jointly carried out by Clay Technology AB in Sweden, VTT Chemical Technology in Finland, Universität Hannover in Germany and Kungliga Tekniska Högskolan in Sweden. Professor Roland Pusch from Clay Technology AB was the co-ordinator of the project. The work in Finland, concentrated on studying the diffusion and porewater chemistry in compacted bentonite, was funded by The European Commission, Posiva Oy and VTT Chemical Technology. The contact person for Posiva Oy was Mr. Jukka-Pekka Salo.

1 INTRODUCTION

In this work, a two-dimensional molecular-level diffusion model for ionic species in compacted bentonite clay has been developed. The modifications to the classical Gouy-Chapman (GC) theory for electrical double layers (EDLs) incorporated into the model stem from the inclusion of various additional features: ionic hydration/dielectric saturation, volume exclusion of ions and charge regulation at the pH-dependent surface hydroxyl sites (specific adsorption).

Hydration effects for ionic species arise in a dielectric continuum, where the dielectric permittivity is treated as a local function of the electric field strength. The hydration of ions is considered in the framework of the Born model (e.g., Bucher and Porter, 1986). The modified Gouy-Chapman (MGC) theory, which includes hydration effects, accounts for the different tendencies of cations of like charge to undergo cation exchange onto the clay surface – a well-known phenomenon that cannot be distinguished by the GC theory. Moreover, a compact Stern layer for physisorbed counter-ions need not be introduced, since the hydration model simulates solvent co-ordination (Pintauro and Verbrugge, 1989).

Contrary to the GC theory, which treats ions as point charges, the present modified theory considers ions as occupying a finite volume in the electrolyte. A practical aspect of this, together with the hydration effect, is that a cation cannot achieve an unphysically high concentration in close proximity to the negatively charged clay surface, which is a major flaw of the GC theory.

Specific adsorption on the bentonite surface is accounted for by using the charge regulation model in which an ionizable surface functionality is able to bind ions from the adjacent solution phase by mechanistic surface complexation. In doing so, the effective surface charge density is assumed to consist of the purely structural and the surface ionizable components in an additive fashion.

The pore geometry of the clay is modelled as an array of non-interconnected tortuous channels with no parallel or serial-type non-uniformities along the pathway. This roughly corresponds to the picture of clay particles of infinite lateral extent aligned in parallel and spaced apart by a constant interlayer distance.

The governing equations for the flux of electrolyte ions through the pore channels are solved by an iterative numerical scheme to relate the characteristics of the flow to the characteristics of the channels and to the composition of the external solution in contact with the clay. In these channels, the equations governing the local ionic equilibrium are numerically integrated on a grid that dynamically adjusts to the prevailing physicochemical conditions. In practical terms, the grid is refined in the proximity of the channel walls.

The computerized model is able to interpret equilibrium and transport experiments for bentonite clays containing different types of background electrolytes at various compactions. The emphasis was on quantifying the extent of co-ion exclusion and on understanding the postulated surface diffusion mechanism on the basis of the well-established EDL theory.

The modified Poisson-Boltzmann solver is capable of calculating the equilibrium com-

position inside a pore channel for any combination of the surface charge density (or surface potential), interlayer spacing and type of electrolyte in contact with the clay. Consequently, it qualitatively explains the experimentally observed cation-exchange selectivities of a clay surface, quantifies co-ion exclusion, accounts for ion-size corrections and ionic hydration, and models pH-dependent adsorption onto the clay by mechanistic surface complexation. Furthermore, by incorporating the EDL theory into the expression for the molecular-level diffusive flux, it is possible to show where the macroscopic flux equation containing a term for surface diffusion stems from. Being able to do this at the *conceptual* level is very important in that surface diffusion in clays has been, and still is, a matter of great controversy and lively debate in the literature.

2 FROM MICROSCOPIC THEORY ...

2.1 Modified Gouy-Chapman (MGC) theory

The expression that forms the basis for all subsequent computation is the electrochemical potential of the jth ion, μ_j (with non-standard terms explicitly identified),

$$\mu_j = \mu_j^0 + kT \ln n_j + Z_j e\psi + \underbrace{A_j/\varepsilon}_{\text{Hydration}} \underbrace{- kT \ln g_j}_{\substack{\text{Volume} \\ \text{exclusion}}} \tag{1}$$

where

$$g_j = 1 - \sum_k \upsilon_{jk} n_k \tag{2}$$

μ_j^0 is the standard state potential, k and T (= 298 K) have their usual meanings, n_j, Z_j and A_j are the number density, valence and hydration parameter of the jth ion, e is the proton charge, ψ is the electrostatic potential, ε is the relative dielectric permittivity, and υ_{jk} is the excluded volume, i.e., the volume around an ion k, which is inaccessible to an ion j (Sparnaay, 1972; Paunov *et al.*, 1996). For interacting double-layers, Paunov *et al.* (1996) suggested that υ_{jk} are eight times the volume of the hydrated counterion in a symmetric electrolyte. In the present analysis, however, we adopt the functional form given by Sparnaay (1972), $\upsilon_{jk} = \frac{2}{3}\pi(r_j + r_k)^3$, where r_j is the hydrated radius of the jth ion, and assume equal sizes for all ions, that is, $r_j = r_k = r$. This results in $\upsilon_{jk} = \upsilon = 4v$, where v is the ionic volume. The hydration parameter, A_j, is calculable from (Gur *et al.*, 1978)

$$A_j = -\Delta H_j \frac{\varepsilon_b}{\varepsilon_b - 1} \tag{3}$$

where ΔH_j is the hydration enthalpy and ε_b takes the value 78.46 at 25 °C and 1 atm (Marcus, 1985). Tabulated values for $-\Delta H_j$ and A_j are given in Table 1.

At equilibrium, the electrochemical potential of ion j is the same throughout the system which allows us to set $\mu_j = \mu_{jr}$, where the subscript "r" denotes a suitably chosen reference state. This condition when substituted in Eqn. (1) yields a modified Boltzmann distribution

$$\frac{n_j}{n_{jr}} = \frac{g_j}{g_{jr}} \exp\left[-\frac{Z_j e}{kT}(\psi - \psi_r) - \frac{A_j}{kT}\left(\frac{1}{\varepsilon} - \frac{1}{\varepsilon_r}\right)\right] \tag{4}$$

In order to be able to solve for the electrostatic potential, a relation between the number densities, n_j, and ψ is needed. This is provided by the Poisson equation

$$-\nabla \cdot (\varepsilon \nabla \psi) = \frac{e}{\varepsilon_0} \sum_k Z_k n_k \tag{5}$$

where ε_0 is the permittivity of vacuum. Together Eqns. (4) and (5) constitute the modified Poisson-Boltzmann equation.

Table 1. Hydration parameters for various ions.

Ion	$-\Delta H^{\dagger}$ (kJ mol^{-1})	$A^{\ddagger}$ (kJ mol^{-1})
H^+	1103	1117.2
Li^+	531	537.9
Na^+	416	421.4
K^+	334	338.3
Rb^+	308	312.0
Cs^+	283	286.7
Ca^{2+}	1602	1622.7
Mg^{2+}	1949	1974.2
Sr^{2+}	1470	1489.0
Cl^-	367	371.7
HCO_3^-	384	389.0
NO_3^-	312	316.0
SO_4^{2-}	1035	1048.4

† Marcus, 1997.
‡ Calculated from Eqn. (3).

In the approach adopted here, ε is taken as a function of the electric field strength, $E\ (=-\nabla\psi)$, across the pore channel (Booth, 1951)

$$\varepsilon(E) = n_D^2 + (\varepsilon_b - n_D^2)\frac{3}{\beta E}\left(\coth\beta E - \frac{1}{\beta E}\right), \qquad \beta \equiv \frac{5\mu_w}{2kT}(n_D^2 + 2) \tag{6}$$

where n_D and μ_w are the optical refractive index and dipole moment of water (Marcus, 1985), respectively.

The pertinent boundary condition for symmetry about the midplane of the pore channel (subscript "m") is

$$\left.\frac{d\psi}{dy}\right|_{y=y_m} = 0 \tag{7}$$

where y is the direction normal to the clay surface and $2y_m$ is the interlayer distance (channel width). The charged surface at $y = 0$ is accounted for either by the surface charge (constant or charge-regulation[1]) boundary condition

$$\left.\frac{d\psi}{dy}\right|_{y=0} = -\frac{\sigma}{\varepsilon_0\varepsilon_s} \tag{8a}$$

or the constant surface potential boundary condition

$$\psi|_{y=0} = \psi_s \tag{8b}$$

where σ is the surface charge density (typically $\sigma = -0.125$ C m^{-2} for montmorillonite, the major constituent of MX-80 bentonite) and the subscript "s" denotes a quantity's value at the surface.

[1] See next section.

The different EDL models considered in this study are:

- the simple Gouy-Chapman (GC) theory: $A_j \equiv 0$ (no hydration forces) and $\upsilon \equiv 0$ (ions as point charges),
- the modified GC theory 1 (MGC1): $A_j > 0$ (hydration forces) and $\upsilon \equiv 0$ (ions as point charges), and
- the modified GC theory 2 (MGC2): $A_j > 0$ (hydration forces) and $\upsilon > 0$ [2] (finite-size ions).

To solve for the governing equations (4) to (8), they are first cast to dimensionless form through substitutions $\hat{y} \equiv \exp(-\kappa y)$ and $\hat{\psi} \equiv e\psi/(kT)$, with κ being the reciprocal of the Debye screening length. Thus, $\hat{y}$ dynamically maps the computational domain where $\hat{\psi}$ exhibits fast variation, i.e., the immediate vicinity of the clay surface. The resulting dimensionless set of equations is then numerically solved (by way of iteration) using the finite difference method on equidistant grid nodes and, subsequently, the solution converted back to the original (y, ψ) co-ordinates by employing the inverses of the above transformations (Paunov *et al.*, 1996).

2.2 Specific adsorption on a charge-regulated surface

In this section, account is taken to extend the applicability of the GC and MGC theories to cases where a specific adsorption component is present. Although the montmorillonite surface tends to be more of equal potential than of equal charge density (e.g., Chan *et al.*, 1984; Greathouse *et al.*, 1994), both of the these approximations are fundamentally wrong (Zhmud, 1999). The tendency to act as a constant-potential surface can be shown to result from charge regulation of the surface (Zhmud and Sonnefeld, 1995). By charge regulation we understand the compensatory behaviour of the surface charge on the clay crystallite edges, formed as a result of reactions between surface hydroxyl groups (SOH) and electrolyte ions, to "regulate" the surface potential [see Reiner and Radke (1993) for detailed discussion]. For example, the surface association-dissociation equilibria in Table 2, where K is the equilibrium constant, can be established for a charge-regulated surface in contact with NaCl as the background electrolyte (e.g., Janusz *et al.*, 1997).

Table 2. *Surface chemical equilibria.*

Surface reaction	K
$SOH + H^+ = SOH_2^+$	K_{a1}
$SOH = SO^- + H^+$	K_{a2}
$SOH + H^+ + Cl^- = SOH_2^+Cl^-$	K_{Cl}
$SOH + Na^+ = SO^-Na^+ + H^+$	K_{Na}

[2] υ is taken equal to four times the volume of the hydrated Na^+ ion, $7.8\ 10^{-28}$ m^3.

The specifically adsorbed ions in Table 2 are considered as model analogs of inner-sphere complexes (no solvent molecules interposed between the surface functional group and the adsorbate, that is, the molecules are adsorbed directly at the surface plane).

The surface charge density due to hydroxyl sites, σ_{SOH}, is expressed as

$$\sigma_{SOH} = eN_{SOH}(\theta^{+}_{SOH} - \theta^{-}_{SOH}), \tag{9}$$

Here, N_{SOH} = number of surface hydroxyl groups per unit area and θ^{+}_{SOH} (θ^{-}_{SOH}) = coverage fraction of positively (negatively) charged surface species, defined as

$$\theta^{+}_{SOH} = \frac{c_{SOH_2^+}}{c_{SOH_T}} \tag{10}$$

and

$$\theta^{+}_{SOH} = \frac{c_{SO^-}}{c_{SOH_T}}, \tag{11}$$

where c_j denote molar concentration units ($= n_j / N_A$) and c_{SOH_T} is the total concentration of surface hydroxyls

$$c_{SOH_T} = c_{SOH_2^+} + c_{SOH} + c_{SO^-} + c_{SOH_2^+Cl^-} + c_{SO^-Na^+}. \tag{12}$$

Upon substituting the surface equilibria in Table 2 in Eqn. (9) and dividing through by c_{SOH}, we arrive at the following expression

$$\sigma_{SOH} = eN_{SOH}\frac{K_{a1}c_{H^+,s} - K_{a2}c^{-1}_{H^+,s}}{1 + K_{a1}c_{H^+,s} + K_{a2}c^{-1}_{H^+,s} + K_{Cl}c_{H^+,s}c_{Cl^-,s} + K_{Na}c^{-1}_{H^+,s}c_{Na^+,s}}. \tag{13}$$

Eqn. (13) yields an adsorption isotherm of Langmuir form which assumes no lateral interactions between adsorbed molecules. The effective surface charge density is assumed to consist of the structural, i.e. intrinsic[3], σ_0, and the surface ionizable components in an additive fashion to give

$$\sigma = \sigma_0 + \sigma_{SOH} = \sigma_0 + eN_{SOH}(\theta^{+}_{SOH} - \theta^{-}_{SOH}) \tag{14}$$

In a general case for N surface reactions and M ions, the surface charge density is given by

$$\sigma = \sigma_0 + eN_{SOH}\frac{\sum_{i=1}^{N} K_i \lambda_i \prod_{j=1}^{M} c_{js}^{\nu_{ij}}}{1 + \sum_{i=1}^{N} K_i \prod_{j=1}^{M} c_{js}^{\nu_{ij}}} \tag{15}$$

where

[3] Cationic substitutions chiefly within the tetrahedral layers give rise to the permanent (fixed) negative structural charge, σ_0, and consequent cation-exchange capacity.

$$\lambda_i = \sum_{j=1}^{M} Z_j \nu_{ij} \tag{16}$$

and ν_{ij} is the stoichiometric coefficient for the jth ion in the ith reaction. The formation reaction stoichiometries for the equilibria in Table 2 are shown in Table 3. They can be seen to coincide with the exponents in the denominator of Eqn. (13).

Table 3. *Formation reaction stoichiometries of surface species.*

Surface species	H^+	Na^+	Cl^-
SOH_2^+	1	0	0
SO^-	−1	0	0
$SOH_2^+Cl^-$	1	0	1
SO^-Na^+	−1	1	0

2.3 Diffusion

In this section, a theoretical model is developed for the diffusion of adsorbed spherical Brownian particles (molecules) within an assumed pore structure. An array of tortuous parallel planar surfaces with a uniform charge density is chosen as the model geometry. The Cartesian co-ordinate system is assumed in such a way that the particles are dispersed in a viscous solvent in the finite interlayer domain, $0 \le y \le y_m$, bounded by a solid plane wall at $y = 0$. The diffusion process of interest occurs under the influence of a concentration gradient maintained parallel to the bounding planar wall in the x-direction. The third co-ordinate is made redundant by making the x-axis co-linear with the concentration gradient (Brenner and Leal, 1977).

The case of relevance to the interpretation of a wealth of experimental diffusion results is one where

- the bentonite is in equilibrium with the solution phase of interest, and
- a trace amount of a diffusing solute is concerned (ensuring the applicability of a *linear*, Henry's-law-type adsorption isotherm).

These two prerequisites, expected to be encountered also in the final repository conditions at the time of the canister failure, make it possible to develop a sound macroscopic description of the diffusion in terms of microscopic quantities.

Before proceeding any further with the derivation, let us first define the following useful quantity used extensively in this and subsequent sections,

$$\gamma(\xi) = \frac{n_j(\xi)}{n_{jr}} - 1 \tag{17}$$

where $\xi\,(\equiv y/y_m)$ is the dimensionless distance and $n_j/n_{jr}\,(=1+\gamma)$ is given by Eqn. (4).

The differential diffusion flux of a Brownian particle through a quiescent solvent in a slit-like microchannel is given by (Brenner and Leal, 1977)[4]

$$j_x = D_{||}(\xi)(1+\gamma)G \tag{18}$$

where $D_{||}(\xi)$ is the position-dependent particle diffusivity for motion parallel to the pore wall and $G = -dc_r/dx$. $c_r = c_r(x)$ is subject to the assumption that *local "adsorption" equilibria* prevail along the diffusion path. In the simplest possible case of steady-state transport, G is the macroscopic concentration gradient between the inlet and outlet reservoirs. The electric field gradient, which is induced by the negatively charged pore walls and perpendicular to G, acts to align the permanent solvent dipoles resulting in a reduction in their degrees of freedom in close proximity of the walls. Consequently, this leads to the increase in solvent viscosity, the so-called electroviscous effect. According to the Nernst-Einstein equation, the diffusion coefficient of a spherical particle is inversely proportional to the relative solvent viscosity, η. Therefore, we modify $D_{||}$ to read

$$D_{||}(\xi) = \frac{D_{||,m}}{\eta(\xi)} \tag{19}$$

where $D_{||,m} = D_{||}(\xi = 1)$ can be a function of the solution composition at $\xi = 1$. In the present analysis, any explicit composition-dependencies of $D_{||,m}$ have been ignored, however. We have adopted the functional form suggested by Andrade and Dodd (1951) to calculate η:

$$\eta = 1 + f(\nabla\psi)^2 \tag{20}$$

where f is the viscoelectric coefficient taken to be 5.0 10^{-16} m^2 V^{-2} (Hunter and Leyendekkers, 1978). From the symmetry about the channel midplane, $\eta(1) = 1$.

A theoretical (by the MGC1 theory) reciprocal viscosity profile between negatively charged montmorillonite surfaces at a separation of 2 nm is plotted in Figure 1. The distance of 1 nm represents the symmetry plane, y_m. The curve is seen to monotonically increase from almost complete immobilization (~0%) at $y = 0$ nm to complete mobilization at $y = 1$ nm. Shown in Figure 1 is also the mean reciprocal viscosity, $\langle\eta^{-1}\rangle$, where the averaging operator, $\langle\bullet\rangle$, is defined by

$$\langle\bullet\rangle = \int_0^1 (\bullet)d\xi \tag{21}$$

[4] The notation differs somewhat from that used in Brenner and Leal (1977).

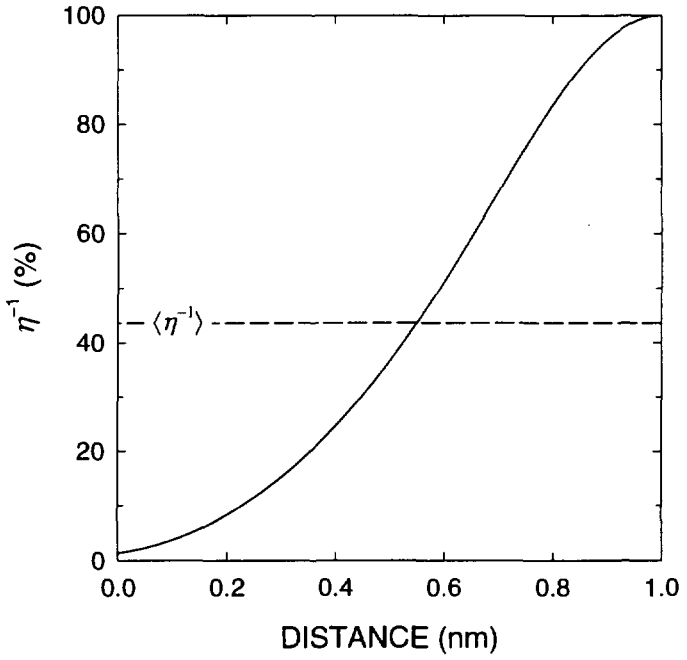

Figure 1. *Calculated (MGC1) reciprocal solvent viscosity as a function of the distance from the negatively charged montmorillonite surface in contact with 0.001 M NaCl.*

On substituting (19) in (18) we have

$$j_x = D_{\|,m}\eta^{-1}(1+\gamma)G \tag{22}$$

To see the effect of the increased solvent viscosity on j_x, we have plotted $\log(1+\gamma)$ and $\log\eta^{-1}(1+\gamma)$ for Na^+, calculated using the MGC1 theory in Figure 2. The area between the two curves corresponds to a decrease of 70% in the effectively mobile sodium concentration. Despite this, all the concentration above the zero level contributes to surface diffusion (see Section 3.2).

As a result of separating the diffusive flux into "bulk" and "surface" contributions, similarly to what has been done here, Brenner and Leal (1977) were able to define the surface diffusivity, D_s, which they claim to be a material property, as

$$D_s = \frac{\langle D_{\|}(\xi)\gamma(\xi)\rangle}{\Gamma} \tag{23}$$

Upon substituting (19) in (23) we have

$$D_s = D_{\|,m}\frac{\langle\eta^{-1}\gamma\rangle}{\Gamma} \tag{24}$$

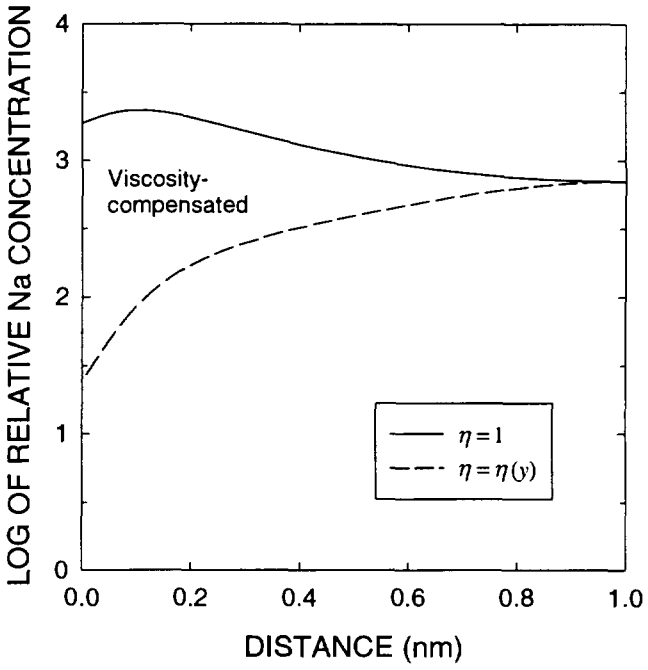

Figure 2. *Calculated (MGC1) logarithm of the relative Na^+ concentration [(—) $\log(1+\gamma)$, (– –) $\log \eta^{-1}(1+\gamma)$] as a function of the distance from the negatively charged montmorillonite surface in contact with 0.001 M NaCl.*

3 ... TO MACROSCOPIC THEORY

3.1 Adsorption

It is only when the system is viewed on a macroscopic or continuum length scale that we have to introduce concepts like adsorption[5] (Brenner and Leal, 1977). From the equation of continuity or by straightforward deduction, we find for the capacity factor, α,

$$\alpha = \phi(1 + \Gamma), \tag{25}$$

where $\Gamma = \langle \gamma \rangle$ is the surface excess per unit area and c_r (the hatched area, ▨, in Figure 3) which is a positive or negative constant for cations and anions, respectively, and nil for neutral molecules (Table 4). The repulsion of anions gives rise to a local deficit (negative surface excess) of anions in the environment of the clay particle in comparison with the equilibrium solution. This deficit has also been termed negative adsorption, which can occur only for species in the diffuse-ion swarm (de Haan, 1964; Sposito, 1989).

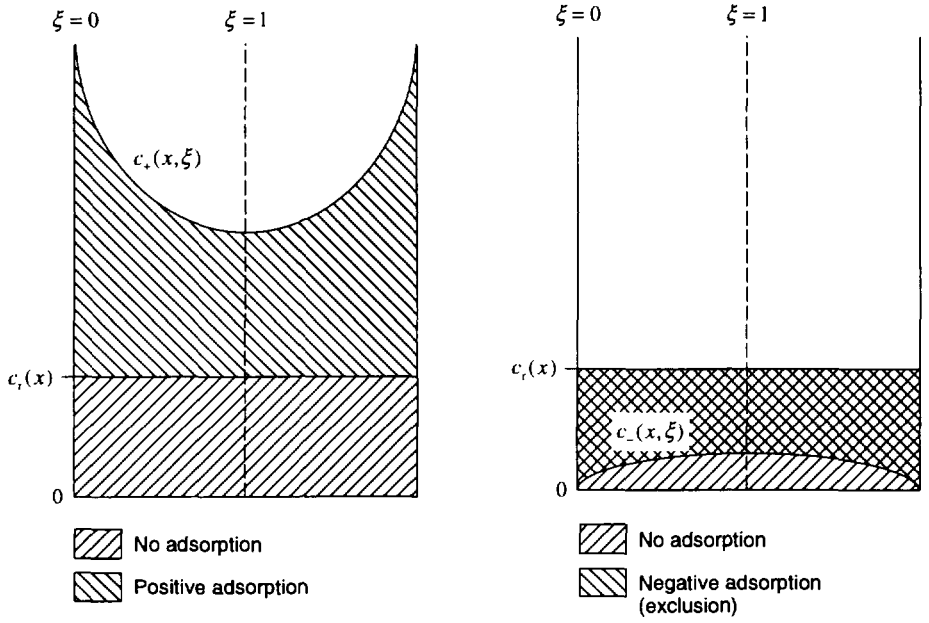

Figure 3. *Schematic view of electrostatic adsorption of cations (left) and anions (right) between negatively charged surfaces for strongly interacting EDLs.*

Table 4. *The sign of Γ and the relative magnitude of α.*

Molecule	Γ	α/ϕ
Anion	$-1 < \Gamma < 0$	$0 < \alpha/\phi < 1$
Neutral	$\Gamma = 0$	$\alpha/\phi = 1$
Cation	$\Gamma > 0$	$\alpha/\phi > 1$

[5] See the IUPAC definition of adsorption (Everett,1972).

On the other hand, α is defined within the macroscopic theory as

$$\alpha = \phi + (1-\phi)\rho K_d, \tag{26}$$

where K_d is the distribution coefficient. From Eqns. (25) and (26) it can be immediately seen that

$$K_d = \frac{\phi\Gamma}{(1-\phi)\rho}, \tag{27}$$

It is important here that K_d, defined in Eqn. (27), readily accounts for the negative adsorption, i.e., exclusion, of co-ions without the need to introduce artificial quantities like the "co-ion porosity"[6]. In the present context, it is thus possible to retain the purely volumetric meaning of the porosity.

So far, we have only considered the adsorption due to the presence of the EDL. In reality, there may be a number of additional sorption mechanisms acting in combination. It is then customary to assume that they may involve different modes of solute attachment, i.e., inner- or outer-sphere surface complex formation, at diverse sorption sites on the solid surface. In this work, these modes and surface sites are collectively described by one generic (inner-sphere) surface functionality, SOH (see Section 2.2). Upon adsorption at the SOH-site, the solute is assumed to be completely immobilized. That is, specific adsorption does not contribute to the diffusion flux. On the other hand, Γ will be modified to read

$$\Gamma \leftarrow \Gamma + \overline{\Gamma} \tag{28}$$

where $\overline{\Gamma}$ stands for the specifically uptaken "surface excess". Consequently, (27) and (26) will appear as

$$K_d = K_{d1} + K_{d2} \tag{29}$$

and

$$\alpha = \alpha_1 + \alpha_2 \tag{30}$$

where

$$K_{d1} = \frac{\phi\Gamma}{(1-\phi)\rho} \tag{31a}$$

$$K_{d2} = \frac{\phi\overline{\Gamma}}{(1-\phi)\rho} \tag{31b}$$

$$\alpha_1 = \phi + (1-\phi)\rho K_{d1} \tag{32a}$$

$$\alpha_2 = (1-\phi)\rho K_{d2} \tag{32b}$$

Thus, α_1 and α_2 can be viewed, in a broad sense, as the capacities related to the mobile and immobile concentrations respectively. Imposing the viscosity correction on K_{d1} yields the so-called transport-K_d. From the assumption that the total adsorption is of

[6] Equal to α for anions ($0 < \alpha < \phi$ in Table 4).

Henry's-law type, it follows that $\overline{\Gamma}$, too, conforms to the linear adsorption isotherm.

3.2 Diffusion

The macroscopic diffusion flux may be related to the characteristics of the porous medium by

$$J_x = \phi\tau^{-2}\langle j_x\rangle = \phi\tau^{-2}D_{\mathrm{II,m}}\langle\eta^{-1}(1+\gamma)\rangle G \tag{33}$$

where ϕ stems from the fact that the active cross-sectional surface area of the porous medium is proportional to the porosity, and τ is the tortuosity factor accounting for the longer tortuous path the molecules have to travel in directions that do not coincide with the direction of the macroscopic concentration gradient. Introducing η into Eqn. (33) as a function of location accounts for a zone of shear rather than a plane of shear (Hiemenz, 1986). The compact Stern layer may be viewed as the extension from the plane wall where η^{-1} exhibits significant deviation from unity. The dimension of this extension is of the order of the size of a water molecule. The theoretical values for $\langle\eta^{-1}\rangle$ close to the surface (not shown) are in agreement with recent electrokinetic investigations where ionic mobilities in the hydrodynamically stagnant Stern layer are of the same order of magnitude as those in the bulk solution (Lyklema and Minor, 1998; Lyklema *et al.*, 1998; Werner *et al.*, 1998).

The first sum term of Eqn. (33) includes the effects arising from the pore shape (i.e., tortuosity) and increased viscosity. It thus represents the situation where a hypothetically discharged solute diffuses between charged parallel plates. It is of interest to note that the geometry factor, experimentally determined for a neutral solute (like tritiated water, HTO), is not strictly due to the pore geometry alone. It also includes drag effects that act on the diffusion coefficient. This is the motivation for defining the pore diffusivity, D_p, as

$$D_\mathrm{p} = \tau^{-2}D_{\mathrm{II,m}}\langle\eta^{-1}\rangle \tag{34}$$

In practical applications, one usually assumes that

$$D_{\mathrm{II,m}} = D_\mathrm{w} \tag{35}$$

where D_w is the diffusivity in a free phase. With (34), Eqn. (33) can be recast in the form

$$J_x = D_\mathrm{e}G \tag{36}$$

where the effective diffusivity, D_e, is defined as

$$D_\mathrm{e} = \phi D_\mathrm{p}(1+q) \tag{37}$$

and

$$q = \frac{\langle\eta^{-1}\gamma\rangle}{\langle\eta^{-1}\rangle} \tag{38}$$

can be understood as a kind of a viscosity-reduced "surface excess". Conceptually, the

areas ▨ and ▧[7] in Figure 3 can be assigned to the pore diffusion (ϕD_p) and surface excess ($q\phi D_p$) contribution to D_e respectively. From Eqn. (37), it is obvious that D_e is an operational quantity. The effective diffusivity, if only a matter of definition, should be used with great care, however, since incorporating concentration effects into it may lead to a situation where D_w is exceeded.

Under the circumstance of linear adsorption, the apparent diffusivity, D_a, is given by

$$D_a = \frac{D_e}{\alpha} \tag{39}$$

Substituting D_e from Eqn. (37) and α from Eqn. (25) in (39) yields

$$D_a = \frac{1+q}{1+\Gamma} D_p \tag{40}$$

In order that D_e calculated from Eqn. (39) be valid, the experiments to determine D_a and α independently of each other should be performed on a similar system. For example, D_a and α measured on a compacted and loose bentonite sample, respectively, are generally not an appropriate set of data for calculating D_e in either compacted or loose sample. Even at its very best, D_e calculated from knowledge of D_a and α can only provide indirect evidence for surface diffusion. Direct support for surface diffusion would necessarily require carefully conducted steady-state experiments with due consideration for the filter-plate effect (Section 4.2.4).

Judging by the mathematical appearance, the separation of the flux equation according to Eqn. (37) in two components (1 and q) is in support of the following macroscopic definition of D_e:

$$D_e = \phi D_p + (1-\phi)\rho K_d D_s \tag{41}$$

rather than its truncated form, $D_e = \phi D_p$. From Eqns. (37), (41) and (27), a simple relation between D_s and D_p is obtained

$$D_s = \frac{q}{\Gamma} D_p. \tag{42}$$

which, apart from the viscosity correction, takes on exactly the same form as D_s defined in Brenner and Leal (1977) for a straight channel ($\tau = 1$). The sign of q for negative ψ is the same as that of Z and is thus indicative of the surface diffusion [understood here as the increase in diffusion flux in relation to the first sum term in Eqn. (37)], and the ion exclusion of cations and anions respectively. q can be seen to vanish for $Z = 0$. Therefore, the proposed decomposition of the flux equation into two components according to Eqn. (37) yields a consistent macroscopic conceptualization for anions, cations and electrically neutral molecules.

Defining the mobile fraction of the capacity, ζ, as

---

[7] Strictly speaking, this area corresponds to the case (GC, $\eta = 1$). For a more general case, (MGC, $\eta > 1$), the half-area could be like that below the dashed line in Figure 3.

$$\zeta \equiv \frac{\alpha_1}{\alpha} \tag{43}$$

it can be easily shown that the effective and apparent diffusivities become, respectively,

$$D_e = \alpha\zeta D_p \tag{44}$$

and

$$D_a = \frac{D_e}{\alpha} = \zeta D_p, \tag{45}$$

where the pore diffusivity is now given by

$$D_p = \tau^{-2} D_w. \tag{46}$$

A comparison of (46) with (34) reveals that τ includes the effect of increased viscosity. The diffusion data for HTO is commonly used to probe structural features of porous media. For the present geometry, this means that the HTO data essentially provides a measure of τ according to

$$\frac{D_{a,HTO}}{D_{w,HTO}} = \tau^{-2}. \tag{47}$$

From Eqns. (45)-(47) we find

$$\zeta = \frac{D_{w,HTO}}{D_{a,HTO}} \frac{D_a}{D_w}. \tag{48}$$

For purely electrostatically adsorbed solutes, $\zeta = (1+\gamma)/(1+\Gamma)$. To this end, for surface diffusion to exist, $\alpha_1 > \phi$.

4 RESULTS AND DISCUSSION

4.1 Ionic equilibria

4.1.1 MGC theory

Figure 4 depicts the calculated electrostatic potential for the three EDL models as a function of the distance from the negatively charged montmorillonite surface immersed in 0.001 M NaCl electrolyte. The distance of 1 nm represents the interlayer half-distance, y_m[8]. The model prediction according to the MGC1 theory leads to a more negative potential than that given by the GC theory over the entire interlayer separation. The interaction of EDLs, and, consequently, the extent of anion exclusion, are reduced with the addition of the salt (not shown). The local maximum in the concentration curve for Na^+ (MGC1) is to be noted in Figure 5. This is important in that the cations are not bound to attain unphysically high concentrations in close proximity to the surface with large absolute values of σ, which can be the case with the GC theory. The orientation of the solvent dipoles[9], induced by the varying electric field, gives rise to the relative dielectric permittivity profile in Figure 6. It is clear from this figure (and intuitively) that the use of the "bulk" (or the zero-electric-field-strength) value for ε is far from being judicious. For interacting double layers, it is valid only at the midpoint between clay platelets.

When the finite size of ions is also explicitly taken into consideration (MGC2), we arrive at the electrostatic potential profile in Figure 4. The effect of volume exclusion is to increase the EDL interaction (and anion exclusion) further. This leads to a substantially flattened concentration distribution for sodium (Fig. 5) and somewhat lower dielectric permittivity over the interlayer separation (Fig. 6) in comparison with the MGC1 theory.

Figure 7 depicts the calculated (MGC2) individual components of $\ln(c/c_r)$ for Na^+. It can be seen that both dielectric saturation and volume exclusion (entropic contribution) are of a repulsive nature.

The calculated ionic concentrations in montmorillonite clay equilibrated with a 0.005 M chloride medium having equal amounts of respective cations are presented in Figure 8. According to the GC theory, the behaviour of the EDL in a mixture of chlorides of the alkali metals is independent of the type of ions, that is, the profiles for all cations are identical (Fig. 8). However, the concentration distributions according to the MGC1 theory become different for each type of ion. The physisorption of these cations can be found to increase according to the well-known selectivity sequence: Li < Na < K < Rb < Cs. On approaching the clay surface the hydration effects start to play a significant role. This is indicated by the onset of deviation between the concentration distributions for cations of like charge at about 0.7 nm.

---

[8] This value is used in all subsequent calculations mainly to demonstrate the significance of MGC effects near the mineral surface.

[9] From complete parallel alignment at $E \to \infty$ to random alignment at $E = 0$.

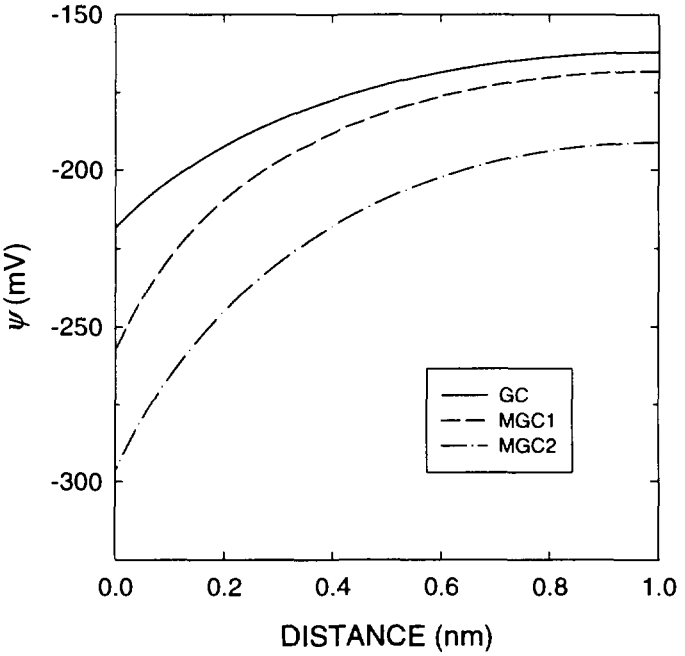

Figure 4. *Electrostatic potential as a function of the distance from the negatively charged montmorillonite surface in contact with 0.001 M NaCl predicted by the GC, MGC1 and MGC2 models.*

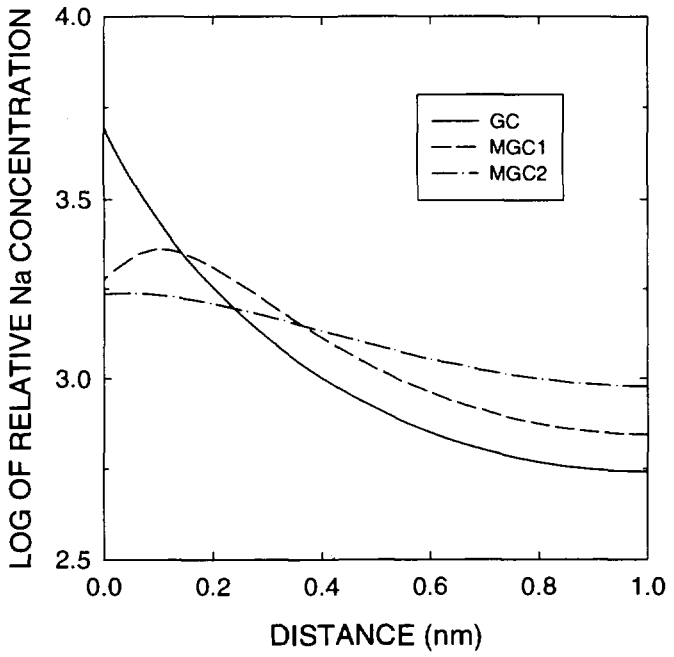

Figure 5. *Logarithm of the relative Na^+ concentration as a function of the distance from the negatively charged montmorillonite surface in contact with 0.001 M NaCl predicted by the GC, MGC1 and MGC2 models.*

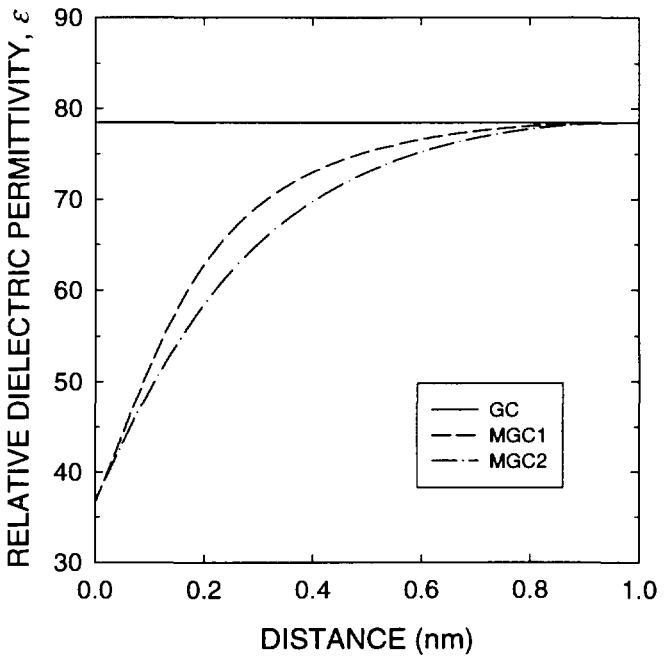

Figure 6. *Relative dielectric permittivity as a function of the distance from the negatively charged montmorillonite surface in contact with 0.001 M NaCl predicted by the GC, MGC1 and MGC2 models.*

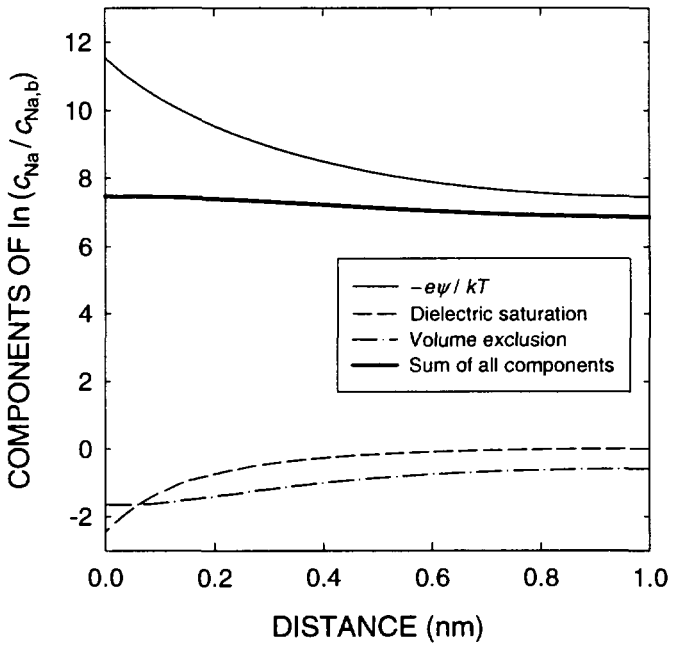

Figure 7. *Individual components of ln (c/c_r) for Na^+ as a function of the distance from the negatively charged montmorillonite surface in contact with 0.001 M NaCl calculated with the MGC2 model.*

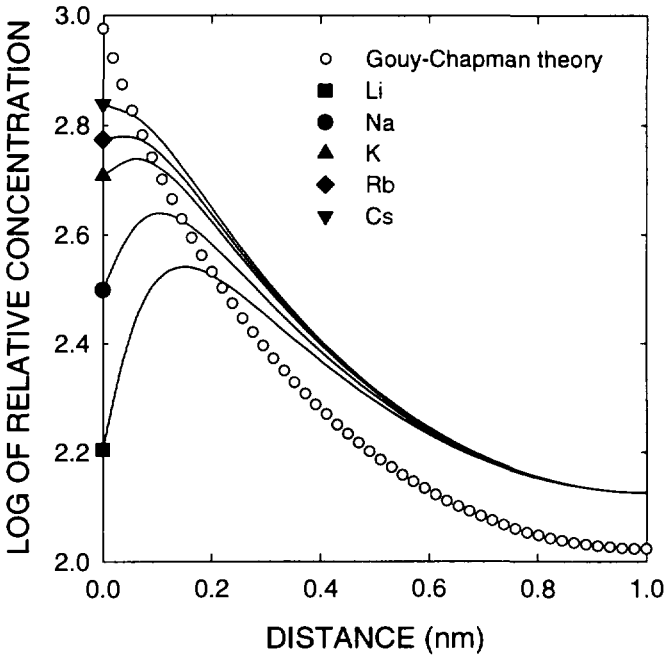

Figure 8. *Logarithmic relative cationic concentrations as a function of the distance from the negatively charged montmorillonite surface in contact with a 0.005 M chloride medium having equal amounts of respective cations.*

4.1.2 Specific adsorption

Figure 9 depicts the calculated (MGC1) effect of the pH variation in the external 0.001 M NaCl solution on the equilibrium concentration profile for sodium. In this model problem, only the association and dissociation reactions of protons with surface ionizable groups have been considered. The number of these groups, N_{SOH}, was chosen to constitute *ca.* 10% of the total clay surface charge at pH 7. The acidity constants, K_{a1} and K_{a2}, were taken from Wieland *et al.* (1994). The resulting point of zero surface charge, pH_{pzc}, for the SOH functionality is 6.05. At this pH, only σ_0 contributes to the effective surface charge. Below and above pH_{pzc}, the surface becomes less and more negative, respectively, than σ_0. From Figure 9, it can be seen that the effective surface charge density decreases (judged by the increased electrostatic adsorption of sodium, for example) with the increasing pH of the external NaCl solution. This is due to the increased concentration of the deprotonated surface species, SO^-.

Here, SOH has been taken as a generic group to jointly represent a number of ionizable surface sites. However, it is straigthforward to extend the approach to take account of more than only one hydr(oxide) site. For example, it is known that montmorillonite edges carry two types of surface ionizable groups with distinctly different affinities for electrolyte ions. Denoting these groups by SiOH and AlOH, Eqn. (9) yields for the acid-base equilibria (analogous to the first two reactions in Table 2)

$$\sigma = \sigma_0 + \sum_M \sigma_{MOH} = \sigma_0 + e\sum_M N_{MOH}(\theta^+_{MOH} - \theta^-_{MOH}) \qquad (49)$$

with

$$\theta^{+}_{\mathrm{MOH}} = \frac{c_{\mathrm{MOH}^{+}_{2}}}{c_{\mathrm{MOH_T}}}, \tag{50}$$

$$\theta^{-}_{\mathrm{MOH}} = \frac{c_{\mathrm{MO}^{-}}}{c_{\mathrm{MOH_T}}}, \tag{51}$$

$$c_{\mathrm{MOH_T}} = c_{\mathrm{MOH}^{+}_{2}} + c_{\mathrm{MOH}} + c_{\mathrm{MO}^{-}}, \tag{52}$$

and $\mathrm{M} = \mathrm{Si, Al}$.

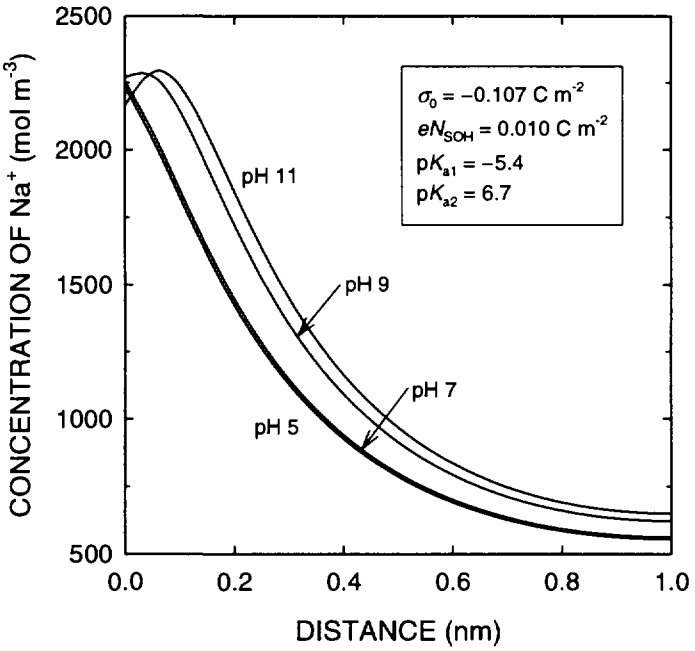

Figure 9. *Na^{+} concentration as a function of the distance from the negatively charged montmorillonite surface in contact with 0.001 M NaCl at a pH from 5 to 11.*

4.1.3 GMM geometry

According to the GENERAL MICROSTRUCTURAL MODEL (GMM) proposed by Pusch *et al.* (1990), the microstructure contributing to ionic transport in compact smectitic clays can be modelled as an array of non-interconnected parallel capillaries with periodic step changes in diameter (Fig. 10). Here, it is of interest to calculate equilibrium ionic distributions within the representative element volume (REV) subtended by the dashed lines in Figure 10 subject to the indicated boundary conditions and variations in the ratios L_2/L_1 and D_2/D_1. Pertinent channel dimensions for MX-80 bentonite compacted to three bulk densities are shown in Table 5. Noteworthy here is the explicit distinction between the basal siloxane (① and ③) and edge amphoteric surfaces (②) at the microstructural level.

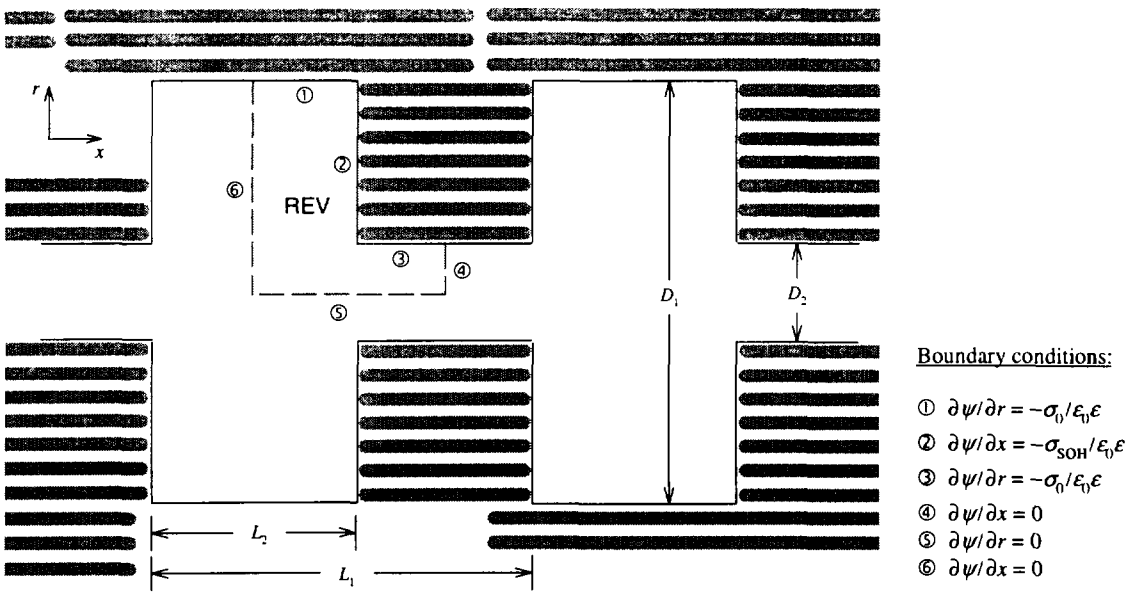

Figure 10. *Pore geometry in the GMM (Pusch et al., 1990). The grey horizontal bars represent clay unit platelets. The area subtended by the dashed lines constitutes the Representative Element Volume (REV).*

Table 5. *Estimated channel dimensions (Pusch, 1999).*

Bulk density (kg m^{-3})	D_1 (nm)	D_2 (nm)	L_1 (nm)	L_2 (nm)
2130	5	1	10	5
1850	10	2	20	10
1570	50	3	100	50

Figure 11 depicts calculated equilibrium anion concentrations in a REV for the bulk density of 2 130 kg m^{-2} and 0.001, 0.01 and 0.1 M uni-univalent electrolyte subject to the assumption that the surface charge density due to broken bonds at crystallite edges (②) constitutes *ca.* 10% of the total negative charge of the clay. Due to electrostatic repulsion, anions are fairly effectively excluded from the pore space beyond $D_2/2$ (blue) in the radial direction and are confined within the central part of the pore (red and yellow) for the 0.001 M solution. It is the opposite for cations, the majority of which can be found in the proximity of the clay surfaces. Upon increasing the solution ionic strength to 0.1 M, a greater part of the pore space becomes accessible to anions (red and yellow) and, consequently, the larger voids begin to act as dead-ends from the viewpoint of anion transport in the x-direction. In general, the critical parameter expected to exert strongest control on the mass transport of anions through the clay is the dimension of the neck, D_2. This is clearly seen in Figure 11, where, at low ionic strengths, the pore neck prevents anions from entering the larger void.

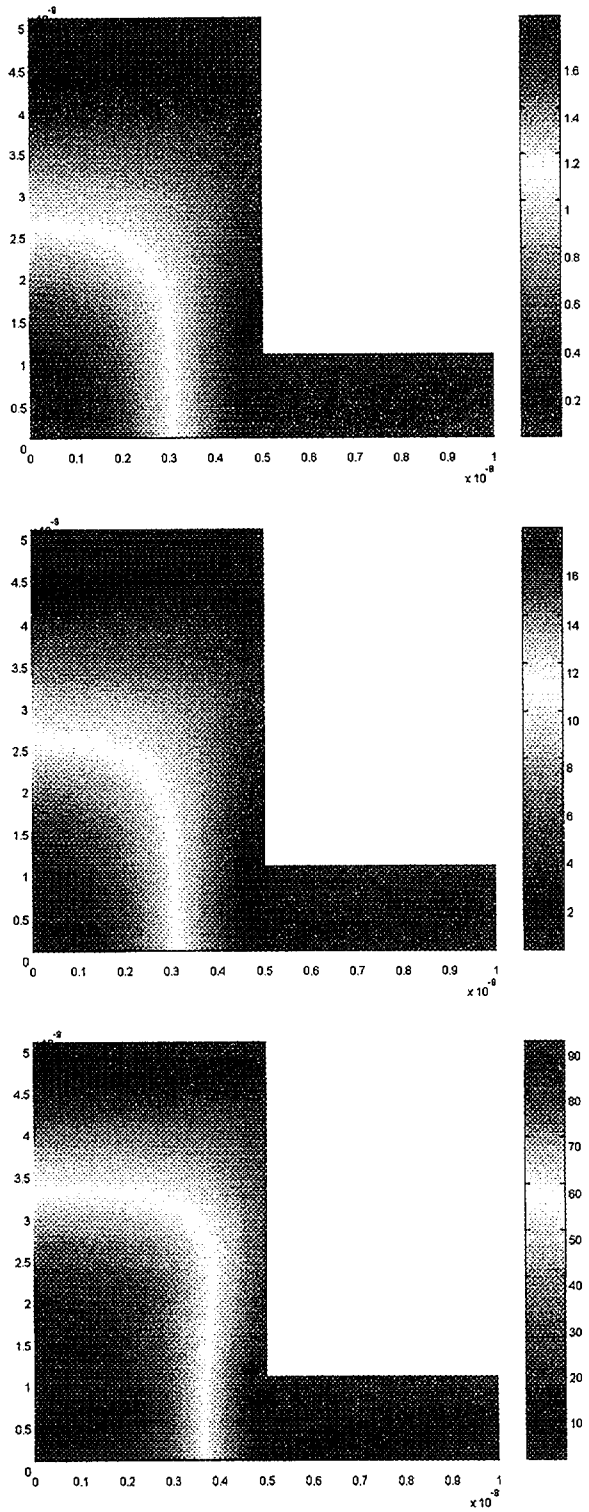

Figure 11. *Relative monovalent anion concentration (%) in a REV for equilibrating 0.001 M (top), 0.01 M (middle) and 0.1 M (bottom) uni-univalent electrolyte. The dimensions pertain to MX-80 bulk density of 2 130 kg m^{-3} in Table 5. Notice the different scales in the colour maps. The GC calculations have been carried out using the MATLAB® Partial Differential Equation Toolbox (MathWorks, 1999).*

4.2 Diffusion

4.2.1 General considerations

The case where the second term in Eqn. (41) has been dropped is quite commonly adopted for the interpretation of diffusion data regardless of the ion's adsorption mechanism. This situation is equivalent to $q = 0$ in Eqn. (37). There are basically two possibilities to realize this condition: (i) by ignoring the increase in counter-ion concentration in the vicinity of negatively charged surfaces, or (ii) by considering the counter-ion in the EDL immobilized. The first possibility is valid only for very thin double layers in relation to the channel half-width (no EDL interaction). However, for, say, a homogenous clay sample whose pores may well be characterized by a channel width of a few nanometres or less, this possibility can be readily ruled out. As to the second possibility, the majority of counter-ions bound only by electrostatics (on the macroscopic scale) can hardly be thought of as taking on fixed positions in the diffuse layer and not responding to the electrochemical gradient in the x-direction. Therefore, the case $q \neq 0$, is in concordance with the physical picture of the EDL. Consequently, this also substantiates the use of the second term in Eqn. (41) as a simple mathematical means of correcting the EDL surface excess to be mobile. In fact, this should be obvious from the very nature of the diffuse double layer.

From Eqn. (37), it can be immediately seen that the increase (decrease) in diffusion flux stems from the increased (decreased) cation (anion) concentration. It is just this increase in flux that is usually referred to as surface diffusion, a subject of great controversy and lively debate in the literature.

When applying Eqn. (41) it is usually assumed that $K_d = 0$ for anions. This may lead to a very common situation where co-ion exclusion is explained by introducing, for example, the "effective co-ion porosity" which is lower than ϕ (see footnote 6) and dependent on the solution ionic strength. However, if ϕ is considered a volumetric property, we have to accept the negative sign of K_d for anions to maintain consistency for anions, cations and neutral solutes. Furthermore, the surface diffusion, understood in the present context as the transport of ions in the EDL, becomes an anion property, too, through the fact that $K_d \neq 0$ for anions. This is perfectly logical since there is no reason as to why anions could not diffuse in the EDL although their concentrations there are very low.

Equation (26) misleadingly fixes the concentration in excess of c_r onto the substrate matrix [through $(1-\phi)\rho K_d$] irrespective of the actual adsorption mechanisms, which may well be one cause of misconception about surface diffusion. Perhaps a more serious source of misunderstanding arises from the belief that two diffusion fluxes (one for the surface and one for the free solution) act in parallel, in such a way that cations close to the surface diffuse much more rapidly than those in the free solution. Rather, upon writing the diffusion flux as

$$J_x = -\phi D_p \frac{\partial (1+q) c_r}{\partial x}, \tag{53}$$

the role of the concentration to enhance the diffusive flux for cations becomes obvious. In this fashion, the rather common misconception that the increase in cation flux is at-

tributable to some phenomenological diffusion constant can hopefully be avoided.

The issue of surface diffusion is closely linked to the adsorption mechanisms involved; the higher the ζ, the more significant the role of surface diffusion.

Figure 12 depicts ζ calculated from Eqn. (48) for Cl^-, Na^+, Cs^+ and Sr^{2+} as a function of clay dry density using diffusion data for purified Japanese Kunipia-F montmorillonite (Kozaki, 1998; Kozaki *et al.*, 1996, 1997, 1998). Also of interest in the results in Figure 12 is the invariance of ζ with dry density for the cations, which, in part, provides support for a linear adsorption isotherm. For Cl^-, which is not supposed to adsorb specifically, the linear decrease in ζ is attributed to a further decrease in τ^{-2} due to anion exclusion (Cl^- must find its way through a more tortuous diffusion pathway than either HTO or cations).

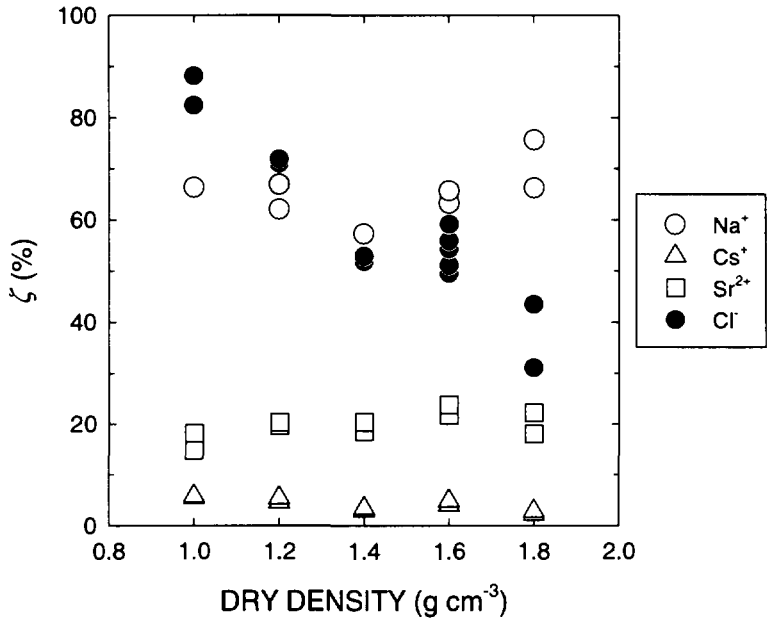

Figure 12. *ζ for Cl^-, Na^+, Cs^+ and Sr^{2+} in Kunipia-F montmorillonite as a function of clay dry density at 25 °C.*

4.2.2 Theoretical results

To gain an idea of the magnitude of the $(1+q)$-term appearing in the expression for D_e, Eqn. (37), Tables 6 and 7 present theoretical values for Na^+ and Cl^-, respectively, for three ionic strengths (0.001, 0.01 and 0.1 M) and three interlayer half-distances (1, 5 and 10 nm) calculated using different EDL models. The results in Table 6 and 7, respectively, indicate a marked increase in surface diffusion and anion exclusion with decreasing ionic strength and interlayer separation. This increase follows the order, GC < MGC1 < MGC2. The results for the MGC2 theory are also shown in graphical form in Figure 13.

Table 6. *Calculated $(1+q)$ for Na^+.*

NaCl	y_m	$1+q$		
(*M*)	(nm)	GC	MGC1	MGC2
0.001	1	791	892	1066
	5	97	100	105
	10	41	44	45
0.01	1	74	89	107
	5	7.6	10.3	10.8
	10	3.5	4.9	5.0
0.1	1	5.8	9.0	10.7
	5	1.3	1.7	1.7
	10	1.1	1.3	1.4

Table 7. *Calculated $(1+q)$ for Cl^-.*

NaCl	y_m	$1+q$		
(*M*)	(nm)	GC	MGC1	MGC2
0.001	1	1.5E-3	1.1E-3	2.4E-4
	5	2.2E-2	1.9E-2	1.6E-2
	10	8.5E-2	6.6E-2	6.1E-2
0.01	1	1.6E-2	1.1E-2	2.4E-3
	5	2.7E-1	1.8E-1	1.6E-1
	10	6.7E-1	4.9E-1	4.7E-1
0.1	1	1.9E-1	1.1E-1	2.8E-2
	5	8.8E-1	7.5E-1	7.3E-1
	10	9.4E-1	8.6E-1	8.5E-1

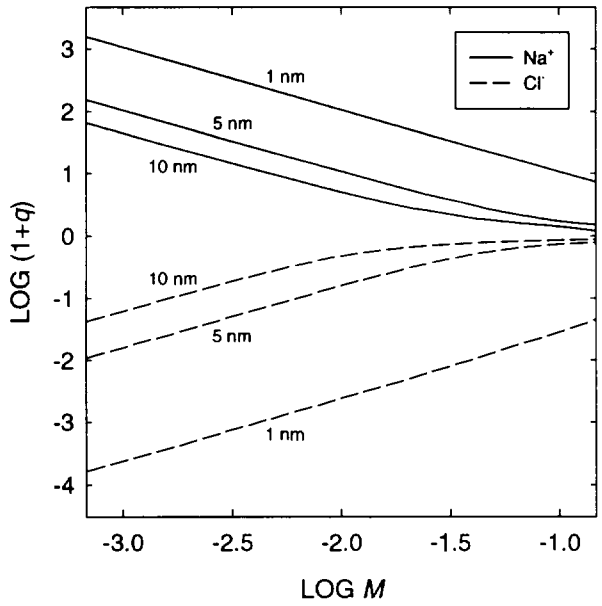

Figure 13. *Calculated (MGC2) log $(1+q)$ for Na^+ and Cl^- as a function of the logarithmic NaCl molarity with y_m taken as a parameter.*

In Tables 8 and 9 are shown theoretical values of $(1+q)/(1+\Gamma)$, present in the definition of D_a in Eqn. (40), corresponding to those in Tables 6 and 7, respectively.

Table 8. *Calculated $(1+q)/(1+\Gamma)$ for Na^+.*

NaCl	y_m	$(1+q)/(1+\Gamma)$		
(*M*)	(nm)	GC	MGC1	MGC2
0.001	1	0.63	0.69	0.83
	5	0.41	0.43	0.44
	10	0.36	0.40	0.39
0.01	1	0.63	0.69	0.83
	5	0.38	0.42	0.43
	10	0.35	0.39	0.39
0.1	1	0.65	0.69	0.83
	5	0.62	0.53	0.54
	10	0.74	0.63	0.64

Table 9. *Calculated $(1+q)/(1+\Gamma)$ for Cl^-.*

NaCl	y_m	$(1+q)/(1+\Gamma)$		
(*M*)	(nm)	GC	MGC1	MGC2
0.001	1	1.28	1.50	1.77
	5	1.19	1.21	1.27
	10	1.12	1.12	1.15
0.01	1	1.27	1.50	1.77
	5	1.20	1.22	1.28
	10	1.11	1.12	1.15
0.1	1	1.26	1.50	1.78
	5	1.10	1.17	1.22
	10	1.05	1.08	1.10

With regard to the theoretical results, there are two points to which further attention should be paid:

- no order-of-magnitude differences among D_a's can be found in particular for $Z = -1$, 0 and 1,
- D_a's are practically independent of the solution ionic strength used and, consequently, of K_d.

Experimental evidence for these points can be found from, e.g., Muurinen (1994), Muurinen *et al.* (1994) and Eriksen and Jansson (1996). Exceptions to the former point are ions that are able to undergo specific binding with the surface. Into this category falls, for example, Cs^+, a prominent part of which may partially dehydrate upon inner-sphere surface complexation [Smith (1998) and references therein]. This amounts to $\zeta_{Cs} << 1$. It should be noted that D_a, defined as the ratio of Eqn. (41) to Eqn. (26), is consistent with the above findings but not the truncated form of Eqn. (41), ϕD_p, divided

by Eqn. (26).

Figures 14 and 15, respectively, show the calculated (MGC2) "equipotential" lines of $\zeta = (1+q)/(1+\Gamma)$ for Na^+ and Sr^{2+} as a function of y_m and the logarithmic NaCl molarity. The results for Cs^+ (not shown) are intermediate between those of Na^+ and Sr^{2+}. It can be seen that ζ possesses a significant channel-width dependence, especially at low y_m where it is also relatively insensitive to changes in the solution ionic strength. It is to be noted that the condition for Na^+ in Figure 12 is realized within the approximate y_m-range from 2.5 nm down to 1.0 nm. Assuming no specific adsorption for Na^+, the 65%-level in Figure 12 is realized at about $y_m = 1.6$ nm. Given this is the proper value for the interlayer half-distance, 90% and 60% of Cs^+ and Sr^{2+}, respectively, should be specifically adsorbed, and thus immobilized on the surface, to explain the ζ-values for these cations in Figure 12. On the other hand, if it is assumed that 32% of sodium is specifically sorbed [Shainberg and Kemper (1966) suggested that this figure is 19-44%; van Schaik *et al.* (1966) found that approximately 70% of exchangeable sodium ions were mobile], the condition $\zeta = 65\%$ is realized at about $y_m = 0.7$ nm. Taking this value as a representative interlayer half-distance, 94% and 83% of Cs^+ and Sr^{2+}, respectively, are needed to account for the ζ-values in Figure 12. The figures, 94% and 83%, are in reasonably good accord with those presented in Khan *et al.* (1994) and Khan *et al.* (1995), respectively, for specifically bound Cs^+ (up to 95%) and Sr^{2+} (85-90%) on bentonite. The agreement between the above y_m-values (0.7-1.6 nm) and the order-of-magnitude estimates for the D_2-dimension (Table 5) is seen to be at least fair. It should be noted that y_m is a decreasing function of the clay dry density.

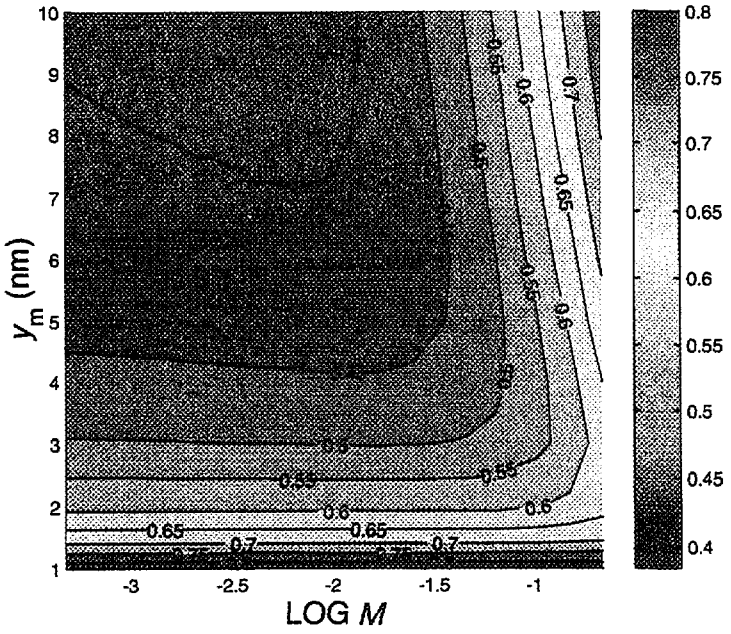

Figure 14. *Calculated (MGC2) contour plot of $(1+q)/(1+\Gamma)$ for Na^+ as a function of y_m and the logarithmic NaCl molarity.*

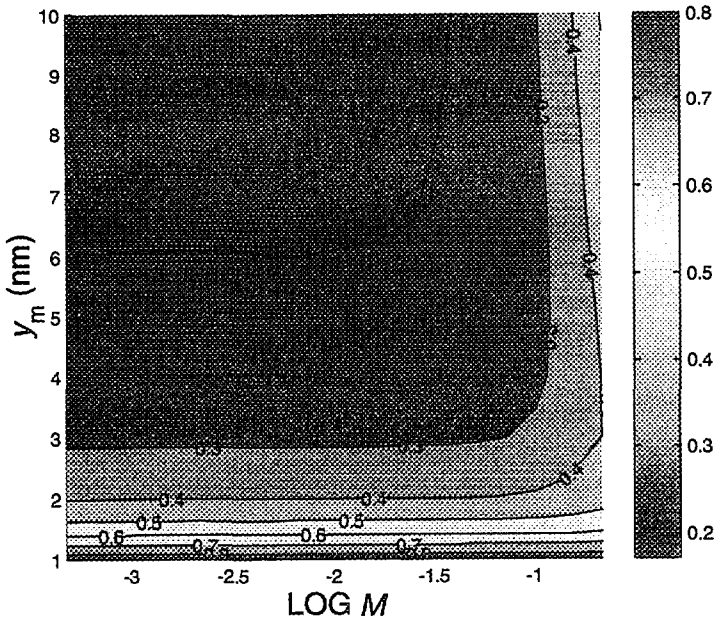

Figure 15. *Calculated (MGC2) contour plot of* $(1+q)/(1+\Gamma)$ *for* Sr^{2+} *as a function of* y_m *and the logarithmic NaCl molarity.*

4.2.3 Effect of filter-plates and the LFD code

In the foregoing analysis, we have omitted the important effect of the filter-plates between which the porous medium (commonly compacted bentonite) is sandwiched in steady-state experiments. They act to decrease the concentration gradient and, consequently, the effective flux of a solute across the medium. In particular, the filter-plate effect should be carefully evaluated when performing and modelling diffusion experiments with cations since transfer through the filter-plates may become the rate-determining process. The influence of the filter-plates has been considered by a number of investigators, e.g., Put (1991), Muurinen (1994) and Eriksen and Jansson (1996). As a convenient check on the soundness of the results obtained, D_e for cations should always be comparable to or greater than $\phi D_{a,HTO}$.

To explicitly account for the filter-plates, we have developed a computerized model, LFD, which runs under the technical computing environment of MATLAB® (MathWorks, 1999) and is basically an enhanced version of the ANADIFF code (Eriksen and Jansson, 1996). The integration of the diffusion equation, as handled in LFD, with pertinent boundary conditions is essentially a four-step procedure:

1. taking the Laplace-transform of the diffusion equation and boundary conditions with respect to time,
2. discretizing the Laplace-transformed diffusion equation and boundary conditions in the spatial dimension using a second-order-accurate finite-difference scheme,
3. solving the matrix equation resulting from step 2 using an algorithm for tridiagonal linear algebraic equations, and

4. taking the numerical inverse Laplace transform of the solution to step 3. The algorithm for the inversion is very robust and efficient.

Steps 1 and 2 are interchangeable. This procedure constitutes the Laplace Transform Finite-Difference (LTFD) technique, which is similar to the Laplace Transform Galerkin (LTG) method described elsewhere (Sudicky, 1990) with the exception of the method used for the spatial discretization.

The LFD code provides significant operational flexibility:

- The filter-plates can be either included or excluded.
- Any combination of Dirichlet (constant concentration) and Neumann (flux) boundary conditions is made possible.
- Arbitrary initial concentration profiles in the sample and filter-plates (resulting, for example, from a previous run) can be defined.
- It is possible to track changes in various quantities (e.g., concentrations, fluxes, etc.) at any future point in time very quickly since very little computational effort is required by the LTFD technique. This is due to the removal of the temporal derivative as a result of taking the Laplace-transform and consequent avoidance of time-steps inherent in time-marching schemes.

The second point has already proven to be very useful in the event that something unexpected takes place during the course of the experiment (Jansson, 1998). These unforeseen occurrences might include a sudden change from a Dirichlet to a Neumann boundary condition, or *vice versa*. A situation of this kind can arise when a solute with a high affinity to the adsorbent surface is present in considerably small amounts on the inlet side, which results in an extremely rapid uptake of the solute and its consequent depletion in the inlet reservoir during the early stage of the experiment. In case one chooses to maintain a Dirichlet boundary condition in such circumstances, an explicit account of the addition of the tracer substance in the feed-side reservoir can be taken using LFD.

The LTFD technique is superior to time-marching schemes not only in view of the CPU time required but also from the vantage point that significant numerical dispersion can be avoided. Contrary to the time-marching schemes, a relatively coarse finite-difference mesh can be employed and no Courant number stability constraints need be imposed (Sudicky, 1990).

A typical example where LFD should find widespread applications is depicted in Figure 16.

A true steady state is attained only when the concentration gradients in both filter-plates are equal, that is, when the depletion rate of the solute in the inlet reservoir equals the rate of influx into the outlet reservoir. However, this condition is never realized in a situation such as that depicted in Figure 16.

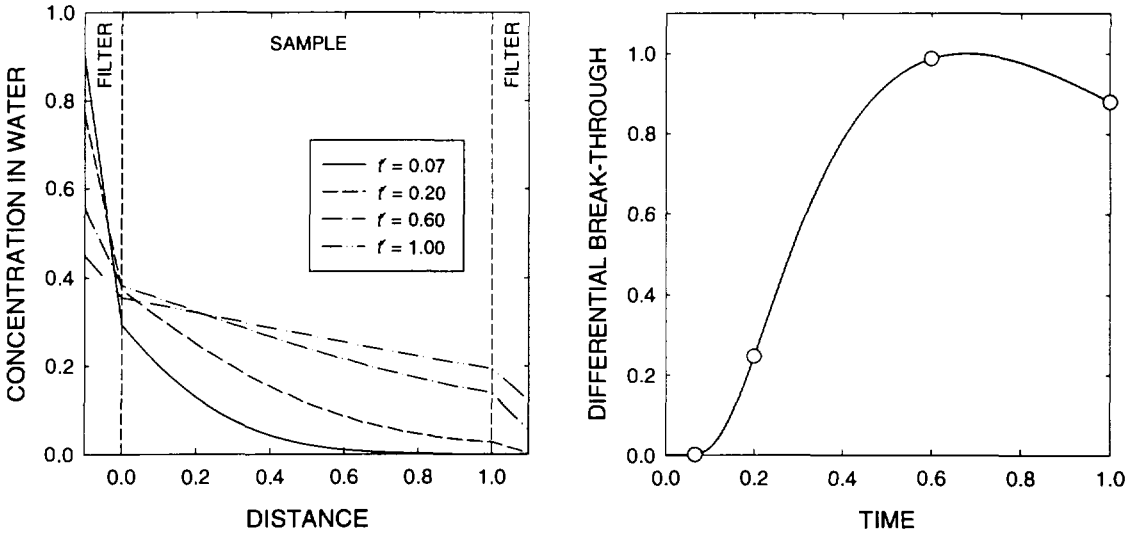

Figure 16. *Diffusion through a porous sample sandwiched between two filter-plates.* ***Left:*** *The concentration in water (or the reference concentration, c_r) at four points in dimensionless time, t'. The concentration in the finite inlet reservoir, imagined to be in contact with the filter-plate on the left-hand side, is initially held at unity. The filter-plates, the sample and the finite outlet reservoir are initially free from the solute. Neumann boundary conditions are assumed at the filter-reservoir interfaces.* ***Right:*** *Differential break-through. The vertical position of each open circle, which corresponds to $\tau = 0.07, 0.20, 0.60$ and 1.00, is proportional to the concentration gradient in the outlet-side filter-plate. In order not to be restricted to any particular case, all the quantities are made dimensionless.*

4.2.4 Pore size in compacted bentonite

An important issue to bear in mind when making comparisons between theoretical and experimental results for compact clays is the highly dynamic nature of the clay's pore structure. For the present calculations, a strictly unimodal pore-size distribution (psd) was assumed. This is, of course, an oversimplified picture of reality since bentonitic clays are known to exhibit a diversity of pore sizes: chiefly a bimodal psd [(i.e., intra- and inter-particle modes (Pusch *et al.*, 1990)] on a log diameter scale. The interplay between compaction and the ionic strength of the equilibrating solution inherently affects the relative proportions of the two principal modes. Studies known to the authors that have been conducted to elucidate the effect of compaction on these proportions are few (Pusch *et al.*, 1990; Muurinen, 1994). It seems, however, that a reduction in total porosity with increasing compaction takes place at the expense of the inter-particle porosity. The effect of increasing solution ionic strength at a given compaction is to increase the proportion of the inter-particle pores. These observations are of consequence to the solute transport and, therefore, more effort to assess the above findings is obviously called for.

4.3 Limitations and applications

Some limitations inherent in the models developed under the topic include:

- The lack of a distance of closest approach for non-specifically adsorbed ions. This dimension is important in that ions are allowed to approach only up to some specified distance (usually the radii of hydrated ions) from the charged surface. It is, however, relatively easy to incorporate this option into the EDL model.
- A simplified pore geometry. In reality, the pore network can be extremely irregular with relatively large voids between stacks of unit flakes as well as necks that are inherently affected by compaction and expected to exert the strongest control on the transport rates of co-ions through the clay.
- The lack of aqueous phase speciation. From the interpretation point of view, it is important to make sure that the tracer substance of interest is present as an aquo-ion only.
- Contrary to what has been assumed in Section 2.2, the contributions of the different reactive phases are generally not additive but sum in nonlinear ways (Brady and Zachara, 1996). This applies to multi-site adsorption models in general.

No attempt was made to calculate the theoretical diffusion fluxes for ionic species within the pore geometry suggested by the GMM (Section 4.1.3) because it provides limited additional value to the treatment. We preferred to adopt the rule of parsimony (Feibleman, 1972) as the guiding principle here and performed the calculations subject to the pore neck controlling the transport of ions. Accounting for the GMM geometry would complicate the calculations unnecessarily (and substantially increase the computational burden for the scoping calculations) since one should: (i) introduce a number of auxiliary parameters related to the periodic geometry itself; and (ii) take the tensorial character of the diffusivity into consideration by introducing the transverse component, $D_{\perp}$, in addition to $D_{||}$. The results in Figure 11 for a univalent anion are shown just to give a hint of the anion's probable whereabouts as a function of the solution molarity. As already stated in Section 4.1.3, the situation for a cation is opposite to that of an anion: its concentration tends to increase on approaching the pore walls. In case one persists in trying to account for the larger voids, one model worth attention is the macroscopic dead-end porosity type.

With regard to the third point, macroscopic models are capable of accounting for the speciation in the bulk phase but do not explicitly take into consideration the pore dimension and all the co-existing microlevel phenomena in the y-direction. Furthermore, they cannot take account of anion exclusion in a consistent fashion. Introducing an effective anion-porosity, which is lower than the volumetric one (Table 4) for all anions, regardless of their valencies, is not quite enough. Firstly, the anion-porosity for divalent anions should be lower than that for a monovalent anion. Secondly, in order to maintain consistency, a correction to the cation porosity should be imposed, too. Thirdly, the porosity influences the speciation. Lowering the porosity may produce somewhat unexpected results in the speciation. Lastly, by introducing the anion porosity, one tacitly sets, often

unknowingly, a constraint on the electrostatics in the system[10]. The problem is that this constraint is not utilized in any way during the course of calculating the electrostatic variables.

As to the last point, unlike the molecular model, macroscopic surface complexation models lack the contribution from diffuse layer adsorption, i.e., Γ defined in Section 3.1. At low pH, this component may dominate the net adsorption, meaning that the role of EDL adsorption can be very similar to ion exchange, which is included in many macroscopic models.

Despite the limitations listed above, some of which are undoubtedly of a rather fundamental nature, the models developed in this work are believed to capture many of the essential features present in the clay-water systems. They should find applications, for example, in the fields of

- colloidal stability,
- estimating the disjoining pressure between charged surfaces,
- micromechanistic understanding of adsorption phenomena,
- finding plausible order-of-magnitude estimates for effective and apparent diffusivities of ionic species in compacted bentonite, and
- re-interpreting existing diffusion data.

[10] Γ is assigned a specified value.

5 REFERENCES

Andrade, E. N. da C., and Dodd, C. 1951. *Proc. Royal Soc. (London)*, **A204**, 449.

Booth, F. 1951. The dielectric constant of water and the saturation effect. *J. Chem. Phys.*, **19**, 391–394, 1327–1328, 1615.

Brady, P. V., and Zachara, J. M. 1996. Geochemical applications of mineral surface science. In: P. V. Brady (ed.), Physics and Chemistry of Mineral Surfaces, CRC Press, Boca Raton, 307–356.

Brenner, H., and Leal, L. G. 1977. A model of surface diffusion on solids. *J. Colloid Interface Sci.*, **62**, 238–258.

Bucher, M., and Porter, T. L. 1986. Analysis of the Born model for hydration of ions. *J. Phys. Chem.*, **90**, 3406–3411.

Chan, D. Y. C., Pashley, R. M., and Quirk, J. P. 1984. Surface potentials derived from co-ion exclusion measurements on homoionic montmorillonite and illite. *Clays and Clay Minerals*, **32**, 131–138.

de Haan, F. A. M. 1964. The negative adsorption of anions (anion exclusion) in systems with interacting double layers. *J. Phys. Chem.*, **68**, 2970–2977.

Eriksen, T. E., and Jansson, M. 1996. Diffusion of I^-, Cs^+ and Sr^{2+} in compacted bentonite – Anion exclusion and surface diffusion. Report SKB-96-16. 20 p.

Everett, D. H. 1972. IUPAC Division of Physical Chemistry. Manual of samples and terminology of physicochemical quantities and units. Appendix II. Definitions, terminology and symbols in colloid and surface chemistry. *Pure Appl. Chem.*, **31**, 577–627.

Feibleman, J. K. 1972. Scientific method: The hypothetico-experimental laboratory procedure of the physical sciences. Martinus Nijhoff, The Hague, 246 p.

Greathouse, J. A., Feller, S. E., and McQuarrie, D. A. 1994. The modified Gouy-Chapman theory: Comparisons between electrical double layer models of clay swelling. *Langmuir*, **10**, 2125–2130.

Gur, Y., Ravina, I., and Babchin, A. J. 1978. On the electrical double layer theory. II. The Poisson-Boltzmann equation including hydration forces. *J. Colloid Interface Sci.*, **64**, 333–341.

Hiemenz, P. C. 1986. Principles of colloid and surface chemistry, 2nd ed. Marcel Dekker, Inc., New York, 815 p.

Hunter, R. J., and Leyendekkers, J. V. 1978. Viscoelectric coefficient of water. *J. Chem. Soc., Faraday Trans. 1*, **74**, 450–455.

Jansson, M. 1998. Personal communication.

Janusz, W., Kobal, I., Sworska, A., and Szczypa, J. 1996. Investigation of the electrical double layer in a metal oxide/monovalent electrolyte solution system. *J. Colloid Interface Sci.*, **187**, 381–387.

Khan, S. A., R.-U.-Rehman, and Khan, M. A. 1994. Sorption of cesium on bentonite. *Waste Management*, **14**, 629–642.

Khan, S. A., R.-U.-Rehman, and Khan, M. A. 1995. Sorption of strontium on bentonite. *Waste Management*, **15**, 641–650.

Kozaki, T., Sato, H., Fujishima, A., Sato, S., and Ohashi, H. 1996. Activation energy for diffusion of cesium in compacted sodium montmorillonite. *J. Nucl. Sci. Technol.*, **33**, 522–524.

Kozaki, T., Sato, H., Fujishima, A., Saito, N., Sato, S., and Ohashi, H. 1997. Effect of dry density on activation energy for diffusion of strontium in compacted sodium montmorillonite. In: Gray, W. J., and Triay, I. R. (eds.), Scientific Basis for Nuclear Waste Management XX, Mater. Res. Soc. Proc. **465**, 893–900.

Kozaki, T., Fujishima, A., Sato, S., and Ohashi, H. 1998. Self-diffusion of sodium ions in compacted sodium montmorillonite. *Nucl. Technol.*, **121**, 63–69.

Kozaki, T. 1998. Personal communication (HTO diffusion data in Kunipia-F montmorillonite).

Lyklema, J., and Minor, M. 1998. On surface conduction and its role in electrokinetics. *Coll. Surf.*, **A140**, 33–41.

Lyklema, J., Rovillard, S., and De Coninck, J. 1998. Electrokinetics: The properties of the stagnant layer unraveled. *Langmuir*, **14**, 5659–5663.

Marcus, Y. 1985. Ion solvation. John Wiley and Sons Ltd., Chichester, 306 p.

Marcus, Y. 1997. Ion properties. Marcel Dekker, Inc., New York, 259 p.

MathWorks, 1999. The MathWorks, Inc. home page at `http://www.mathworks.com/`.

Muurinen, A. 1994. Diffusion of anions and cations in compacted sodium bentonite. VTT Publications 168. 75 p. + app. 83 p.

Muurinen, A., Lehikoinen, J., and Pusch, R. 1994. Literature study on the microstructure of bentonite and its effect on diffusion. Report YJT-94-22. 80 p. +app. 6 p.

Paunov, V. N., Dimova, R. I., Kralchevsky, P. A., Broze, G., and Mehreteab, A. 1996. The hydration repulsion between charged surfaces as an interplay of volume exclusion and dielectric saturation effects. *J. Colloid Interface Sci.*, **182**, 239–248.

Pintauro, P. N., and Verbrugge, M. W. 1989. The electric-potential profile in ion-exchange membrane pores. *J. Membrane Sci.*, **44**, 197–212.

Pusch, R., Karnland, O., and Hökmark, H. 1990. GMM – A general microstructural model for qualitative and quantitative studies of smectite clays. Report SKB-90-43. 94 p.

Pusch, R. 1999. Personal communication.

Put, M. J. 1991. An improved mathematical model for the interpretation of the flow-through type diffusion tests with influence of filterplates. *Radioactive Waste Management and the Nuclear Fuel Cycle*, **16**, 69–81.

Reiner, E. S., and Radke, C. J. 1993. Double layer interactions between charge-regulated colloidal surfaces: Pair potentials for spherical particles bearing ionogenic surface groups. *Adv. Colloid Interface Sci.*, **47**, 59–147.

Shainberg, I., and Kemper, W. D. 1966. Hydration status of adsorbed cations. *Soil Sci. Soc. Am. Proc.*, **30**, 707–713.

Smith, D. E. 1998. Molecular computer simulations of the swelling properties and interlayer structure of cesium montmorillonite. *Langmuir*, **14**, 5959–5967.

Sparnaay, M. J. 1972. Ion-size corrections of the Poisson-Boltzmann equation. *J. Electroanal. Chem.*, **37**, 65–70.

Sposito, G. 1989. The chemistry of soils. Oxford University Press, New York. 277 p.

Sudicky, E. A. 1990. The Laplace transform Galerkin technique for efficient time-continuous solution of solute transport in double porosity media. *Geoderma*, **46**, 209–232.

van Schaik, J. C., Kemper, W. D., and Olsen, S. R. 1966. Contribution of adsorbed cations to diffusion in clay-water systems. *Soil Sci. Soc. Am. Proc.*, **30**, 17–22.

Werner, C., Körber, H., Zimmermann, R., Dukhin, S., and Jacobasch, H.-J. 1998. Extended electrokinetic characterization of flat solid surfaces. *J. Colloid Interface Sci.*, **208**, 329–346.

Wieland, E., Wanner, H., Albinsson, Y., Wersin, P., and Karnland, O. 1994. A surface chemical model of the bentonite-water interface and its implications for modelling the near field chemistry in a repository for spent fuel. Report SKB-94-26. 64 p.

Zhmud, B. V. 1999. At `http://www.surfchem.kth.se/yki/borisz/www/dbllay.htm`

Zhmud, B. V., and Sonnefeld, J. 1995. Charge regulation at the surface of porous silica. *J. Chem. Soc., Faraday Trans.*, **91**, 2965–2970.

POSIVA REPORTS 1999, situation 3/99

POSIVA 99-01
Measurement of thermal conductivity and diffusivity in situ: Literature survey and theoretical modelling of measurements
Ilmo Kukkonen, Ilkka Suppala
Geological Survey of Finland
January 1999
ISBN 951-652-056-1

POSIVA 99-02
An overview of a possible approach to calculate rock movements due to earthquakes at Finnish nuclear waste repository sites
Paul R. LaPointe, Trenton T. Cladouhos
Golder Associates Inc., Washington, USA
February 1999
ISBN 951-652-057-X

POSIVA 99-03
Site Scale Groundwater Flow in Olkiluoto
Jari Löfman
VTT Energy
March 1999
ISBN 951-652-058-8

POSIVA 99-04
The psychosocial consequences of spent fuel disposal
Jura Paavola, Liisa Eränen
University of Helsinki
Department of Social Psychology
March 1999 (in Finnish)
ISBN 951-652-059-6

POSIVA 99-05
The effects of the final disposal facility for spent nuclear fuel on regional economy
Seppo Laakso
Seppo Laakso Urban Research
March 1999 (in Finnish)
ISBN 951-652-060-X

POSIVA 99-06
Radwaste management as a social issue
Ismo Kantola
University of Turku
Department of Sociology
March 1999 (in Finnish)
ISBN 951-652-061-8

POSIVA 99-07
Safety assessment of spent fuel disposal in Hästholmen, Kivetty, Olkiluoto and Romuvaara – TILA-99
Timo Vieno, Henrik Nordman
VTT Energy
March 1999
ISBN 951-652-062-6

POSIVA 99-08

Final disposal of spent nuclear fuel in Finnish bedrock - Hästholmen site report
Pekka Anttila, Fortum Engineering Oy
Henry Ahokas, Fintact Oy
Kai Front, VTT Communities and Infrastructure
Heikki Hinkkanen, Posiva Oy
Erik Johansson, Saanio & Riekkola Oy
Seppo Paulamäki, Geological Survey of Finland
Reijo Riekkola, Saanio & Riekkola Oy
Jouni Saari, Fortum Engineering Oy
Pauli Saksa, Fintact Oy
Margit Snellman, Posiva Oy
Liisa Wikström, Posiva Oy
Antti Öhberg, Saanio & Riekkola Oy
March 1999 (to be published)
ISBN 951-652-063-4

POSIVA 99-09

Final disposal of spent nuclear fuel in Finnish bedrock - Kivetty site report
Pekka Anttila, Fortum Engineering Oy
Henry Ahokas, Fintact Oy
Kai Front, VTT Communities and Infrastructure
Eero Heikkinen, Fintact Oy
Heikki Hinkkanen, Posiva Oy
Erik Johansson, Saanio & Riekkola Oy
Seppo Paulamäki, Geological Survey of Finland
Reijo Riekkola, Saanio & Riekkola Oy
Jouni Saari, Fortum Engineering Oy
Pauli Saksa, Fintact Oy
Margit Snellman, Posiva Oy
Liisa Wikström, Posiva Oy
Antti Öhberg, Saanio & Riekkola Oy
March 1999 (to be published)
ISBN 951-652-064-2

POSIVA 99-10

Final disposal of spent nuclear fuel in Finnish bedrock - Olkiluoto site report
Pekka Anttila, Fortum Engineering Oy
Henry Ahokas, Fintact Oy
Kai Front, VTT Communities and Infrastructure
Heikki Hinkkanen, Posiva Oy
Erik Johansson, Saanio & Riekkola Oy
Seppo Paulamäki, Geological Survey of Finland
Reijo Riekkola, Saanio & Riekkola Oy
Jouni Saari, Fortum Engineering Oy
Pauli Saksa, Fintact Oy
Margit Snellman, Posiva Oy
Liisa Wikström, Posiva Oy
Antti Öhberg, Saanio & Riekkola Oy
March 1999 (to be published)
ISBN 951-652-065-0

POSIVA 99-11

Final disposal of spent nuclear fuel in Finnish bedrock - Romuvaara site report
Pekka Anttila, Fortum Engineering Oy
Henry Ahokas, Fintact Oy
Kai Front, VTT Communities and Infrastructure
Heikki Hinkkanen, Posiva Oy
Erik Johansson, Saanio & Riekkola Oy
Seppo Paulamäki, Geological Survey of Finland
Reijo Riekkola, Saanio & Riekkola Oy
Jouni Saari, Fortum Engineering Oy
Pauli Saksa, Fintact Oy
Margit Snellman, Posiva Oy
Liisa Wikström, Posiva Oy
Antti Öhberg, Saanio & Riekkola Oy
March 1999 (to be published)
ISBN 951-652-066-9

POSIVA 99-12

Site scale groundwater flow in Hästholmen
Jari Löfman
VTT Energy
March 1999 (to be published)
ISBN 951-652-067-7

POSIVA 99-13

Regional-to-site scale groundwater flow in Kivetty
Eero Kattilakoski, Ferenc Mészáros
VTT Energy
March 1999 (to be published)
ISBN 951-652-068-5

POSIVA 99-14

Regional-to-site scale groundwater flow in Romuvaara
Eero Kattilakoski, Lasse Koskinen
VTT Energy
March 1999 (to be published)
ISBN 951-652-069-3

POSIVA 99-15

Site-to-canister scale flow and transport at the Hästholmen, Kivetty, Olkiluoto and Romuvaara sites
Antti Poteri, Mikko Laitinen
VTT Energy
March 1999 (to be published)
ISBN 951-652-070-7

POSIVA 99-16

Käytetyn ydinpolttoaineen loppusijoituslaitoksen normaalikäytön, käyttöhäiriöiden ja onnettomuustilanteiden aiheuttamien säteilyannosten arviointi
Jukka Rossi, Heikki Raiko, Vesa Suolanen, Mikko Ilvonen
VTT Energy
March 1999 (to be published)
(in Finnish)
ISBN 951-652-071-5

POSIVA 99-17

Käytetyn ydinpolttoaineen kuljetusten terveysriskien arviointi
Vesa Suolanen, Risto Lautkaski, Jukka Rossi
VTT Energy
March 1999 (to be published)
(in Finnish)
ISBN 951-652-072-3

POSIVA 99-18

Design report of the disposal canister for twelve fuel assemblies
Heikki Raiko
VTT Energy
March 1999 (to be published)
ISBN 951-652-073-1

POSIVA 99-19

Estimation of block conductivities from hydrologically calibrated fracture networks - description of methodology and application to Romuvaara investigation area
Auli Niemi[1,2], *Kimmo Kontio*[2],
Auli Kuusela-Lahtinen[2], *Tiina Vaittinen*[2]
[1]Royal Institute of Technology, Hydraulic Engineering, Stockholm
[2]VTT Communities and Infrastructure
March 1999
ISBN 951-652-074-X

POSIVA 99-20

Porewater chemistry in compacted bentonite
Arto Muurinen, Jarmo Lehikoinen
VTT Chemical Technology
March 1999
ISBN 951-652-075-8

POSIVA 99-21

Ion diffusion in compacted bentonite
Jarmo Lehikoinen
VTT Chemical Technology
March 1999
ISBN 951-652-076-6